



Deposited via The University of Leeds.

White Rose Research Online URL for this paper:

<https://eprints.whiterose.ac.uk/id/eprint/146459/>

Version: Accepted Version

Proceedings Paper:

Markovic, U, Früh, N, Aristidou, P et al. (2019) Interval-Based Adaptive Inertia and Damping Control of a Virtual Synchronous Machine. In: Proceedings of the 2019 IEEE PowerTech conference. 2019 IEEE PowerTech, 23-27 Jun 2019, Milan, Italy. IEEE. ISBN: 978-1-5386-4723-3.

<https://doi.org/10.1109/PTC.2019.8810640>

© 2019, IEEE. This conference paper is protected by copyright. Uploaded in accordance with the publisher's self-archiving policy.

Reuse

Items deposited in White Rose Research Online are protected by copyright, with all rights reserved unless indicated otherwise. They may be downloaded and/or printed for private study, or other acts as permitted by national copyright laws. The publisher or other rights holders may allow further reproduction and re-use of the full text version. This is indicated by the licence information on the White Rose Research Online record for the item.

Takedown

If you consider content in White Rose Research Online to be in breach of UK law, please notify us by emailing eprints@whiterose.ac.uk including the URL of the record and the reason for the withdrawal request.

Interval-Based Adaptive Inertia and Damping Control of a Virtual Synchronous Machine

Uros Markovic*, Nicolas Früh*, Petros Aristidou[§], Gabriela Hug*

* EEH - Power Systems Laboratory, ETH Zurich, Physikstrasse 3, 8092 Zurich, Switzerland

[§] School of Electronic and Electrical Engineering, University of Leeds, Leeds LS2 9JT, UK

Emails: {markovic, hug}@eeh.ee.ethz.ch, nfrueh@student.ethz.ch, p.aristidou@leeds.ac.uk

Abstract—This paper presents a novel virtual synchronous machine controller for converters in power systems with a high share of renewable resources. Using an interval-based approach, the emulated inertia and damping constants are adaptively adjusted according to the frequency disturbance in the system, while simultaneously keeping the frequency within prescribed limits. Furthermore, the sufficient stability conditions for control tuning are derived. The proposed design is integrated into a state-of-the-art converter control scheme and tested through time-domain simulations. A comparative study against the existing approaches in the literature verifies the control effectiveness.

Index Terms—virtual synchronous machine (VSM), voltage source converter (VSC), swing equation, adaptive control

I. INTRODUCTION

In the light of evergrowing integration of renewable energy sources as well as the current trends of phasing-out traditional synchronous generators, the problems associated to low-inertia systems are becoming a reality [1]. The loss of rotational inertia can have devastating effects on system dynamics, with large frequency deviations potentially triggering undesirable events such as load-shedding and large-scale blackouts. With the apparent need for an adequate system-level service, the provision of fast frequency support by grid-scale energy storage devices appears to be a viable solution. Furthermore, such support can be incorporated within an existing control scheme of a *grid-forming* Voltage Source Converter (VSC) [2].

Despite numerous approaches in the literature, almost all VSC control strategies can be formulated as a Virtual Synchronous Machine (VSM) equivalent, an emulation technique based on a swing equation of a synchronous machine [3]. However, a vast majority of such designs assumes an infinite amount of power and energy on the converter’s DC-side, thus neglecting the dynamical limitations of the capacitor, which might be an issue for real-world applications [4]. This problem was addressed in [5] with a distributed virtual inertia approach that regulates the DC-link voltages such that the capacitors are aggregated into a large unit for frequency support. However, it is implemented via a basic proportional frequency controller that limits its responsiveness. Such obstacle is usually resolved with inclusion of a derivative control term corresponding to the Rate-of-Change-of-Frequency (RoCoF) measurement. Several strategies for providing fast frequency regulation based

on the RoCoF signal have been proposed, varying from a simple PD frequency control [6], to more complex heuristic [7] and optimization-based [8]–[10] VSM tuning. Moreover, a subgroup of so-called *interval-based* controllers emerged [11], [12], where a sign of the trigger signal $\rho = (\Delta\omega)(d\omega/dt)$ is used to indicate whether the unit is in the *accelerating* or *decelerating* mode, and subsequently adjust the VSM parameters in a gain-scheduling fashion. Nonetheless, all concepts mentioned above focus solely on the overall frequency improvement, while disregarding the energy resources required for such regulation. We tackle this issue by proposing an *adaptive* VSM control design that simultaneously keeps the frequency within prescribed limits and minimizes the needed control effort.

The contribution of this work is two-fold. First, we present a novel, frequency-constrained adaptive VSM controller using an interval-based approach. Moreover, we derive the sufficient tuning conditions for ensuring stable system operation. Secondly, the proposed VSM strategy is implemented within a state-of-the-art converter control scheme and compared against the existing concepts in the literature.

The remainder of the paper is structured as follows. In Section II, the frequency dynamics of a generic low-inertia system are derived analytically. Section III describes the interval-based adaptive VSM design and proposes a novel formulation, together with the respective stability conditions. Section IV showcases the time-domain simulation results and compares the methods, whereas Section V draws the main conclusions and discusses future work.

II. SYSTEM FREQUENCY DYNAMICS

A. Primary Frequency Control in Low Inertia Systems

The first goal is to derive a simplified, but sufficiently accurate, uniform frequency response model of a low-inertia system. We study a system comprised of *traditional* ($i \in \mathcal{N}_g$) and *converter-based* ($m \in \mathcal{N}_c$) generators as depicted in Fig. 1. The generator dynamics are described by the swing equation, with M_g and D_g denoting the normalized inertia and damping constants corresponding to the Center-of-Inertia (CoI) of the generators. The low-order model proposed in [13] is used for modelling the governor droop and turbine dynamics; T_{g_i} are the turbine time constants, R_{g_i} and K_{g_i} are the respective droop and mechanical power gain factor, while F_{g_i} refers to the fraction of total power generated by the synchronous machine i . Furthermore, we incorporate the

This project has received funding from the European Union’s Horizon 2020 research and innovation programme under grant agreement No 691800. This paper reflects only the authors’ views and the European Commission is not responsible for any use that may be made of the information it contains.

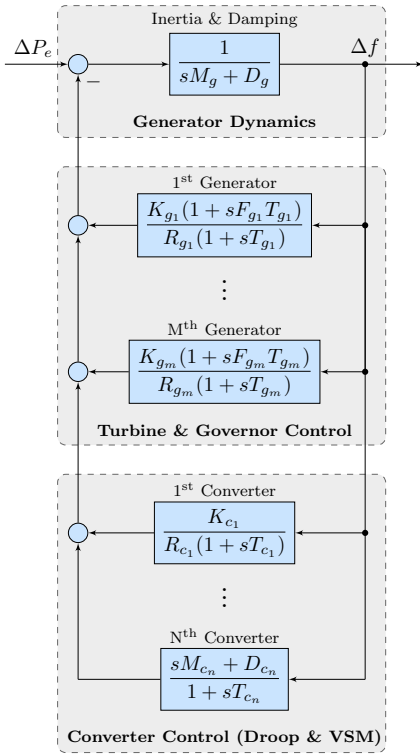


Fig. 1: Uniform system frequency dynamics model.

impact of grid-forming converters, as they are the only type of PE-interfaced units providing frequency support [2], [14]. A particular focus is set on droop ($j \in \mathcal{N}_d$) and VSM-based ($k \in \mathcal{N}_v$) control schemes, as these are two of the currently most prevalent emulation techniques in the literature [15], which in fact have equivalent properties in the forming mode of operation [16]. Here, T_{c_m} are the time constants of the converters, R_{c_j} and K_{c_j} are the respective droop and mechanical power gain factors, whereas M_{c_k} and D_{c_k} denote the normalized virtual inertia and damping constants of VSM converters.

B. Analytic Formulation of Frequency Metrics

From Fig. 1 we can now derive a transfer function $G(s)$ of a general-order system dynamics, as follows:

$$G(s) = \frac{\Delta f}{\Delta P_e} = \left(\underbrace{(sM_g + D_g) + \sum_{i \in \mathcal{N}_g} \frac{K_{g_i}(1 + sF_{g_i}T_{g_i})}{R_{g_i}(1 + sT_{g_i})}}_{\text{traditional generators}} + \underbrace{\sum_{j \in \mathcal{N}_d} \frac{K_{c_j}}{R_{c_j}(1 + sT_{c_j})}}_{\text{droop converters}} + \underbrace{\sum_{k \in \mathcal{N}_v} \frac{sM_{c_k} + D_{c_k}}{1 + sT_{c_k}}}_{\text{VSM converters}} \right)^{-1} \quad (1)$$

Assuming similar time constants ($T_{g_i} \approx T$) of all synchronous machines, usually 2-3 orders of magnitude higher than the ones of converters, justifies the approximation $T \gg T_{c_m} \approx 0$. Now we can transform (1) into the following expression:

$$G(s) = \frac{1}{MT} \frac{1 + sT}{s^2 + 2\zeta\omega_n s + \omega_n^2} \quad (2)$$

where the natural frequency (ω_n) and damping ratio (ζ) are computed as

$$\omega_n = \sqrt{\frac{D + R_g}{MT}} \quad , \quad \zeta = \frac{M + T(D + F_g)}{2\sqrt{MT(D + R_g)}} \quad (3)$$

and the respective parameters M , D , R_g and F_g are computed as weighted system averages described in [10].

Assuming a stepwise disturbance in the electrical power $\Delta P_e(s) = -\Delta P/s$, the time-domain expression for frequency deviation ($\omega(t) \equiv \Delta f(t)$) can be derived as:

$$\omega(t) = -\frac{\Delta P}{MT\omega_n^2} - \frac{\Delta P}{M\omega_d} e^{-\zeta\omega_n t} \left(\sin(\omega_d t) - \frac{1}{\omega_n T} \sin(\omega_d t + \phi) \right) \quad (4)$$

with the introduction of new variables

$$\omega_d = \omega_n \sqrt{1 - \zeta^2} \quad , \quad \phi = \sin^{-1} \left(\sqrt{1 - \zeta^2} \right) \quad (5)$$

The time instance of frequency nadir (t_m) can be determined by observing the RoCoF, i.e., finding the instance at which the derivative of the frequency is equal to zero:

$$\dot{\omega}(t_m) = 0 \mapsto t_m = \frac{1}{\omega_d} \tan^{-1} \left(\frac{\omega_d}{\zeta\omega_n - T^{-1}} \right) \quad (6)$$

Substituting t_m into (4) and conducting a set of mathematical transformations yields the value of frequency nadir as:

$$\omega_{\max} = -\frac{\Delta P}{D + R_g} \left(1 + \sqrt{\frac{T(R_g - F_g)}{M}} e^{-\zeta\omega_n t_m} \right) \quad (7)$$

whereas the maximum RoCoF occurs at the disturbance instance t_0 and is equal to $\dot{\omega}_{\max} = \dot{\omega}(t_0^+) = -\frac{\Delta P}{M}$. Furthermore, the frequency settles at the steady-state value of $\omega_{ss} = \frac{\Delta P}{D + R_g}$. The accuracy of the proposed uniform model in (1)–(7) has already been rigorously investigated and verified in [10].

We can conclude that the frequency metrics of interest are directly dependent on total inertia and damping constants, and can thus be regulated through *adaptive* VSM control gains: RoCoF and steady-state value explicitly as $\dot{\omega}_{\max} \sim M^{-1}$ and $\omega_{ss} \sim D^{-1}$, and nadir through a highly non-linear function $\omega_{\max} = f_{\omega}(M, D)$ given in (7).

III. INTERVAL-BASED ADAPTIVE CONTROL DESIGN

In this section, we explain the general concepts of an interval-based adaptive VSM approach. Moreover, the existing control approaches in the literature are discussed and a new controller with an improved performance is proposed, together with the sufficient stability conditions.

A. Theoretical Concept

Let us observe a frequency response to a step disturbance described in (4) and illustrated in Fig 2. The system response consists of alternating *accelerating* and *decelerating* intervals, similar to the power-angle curve of a typical synchronous

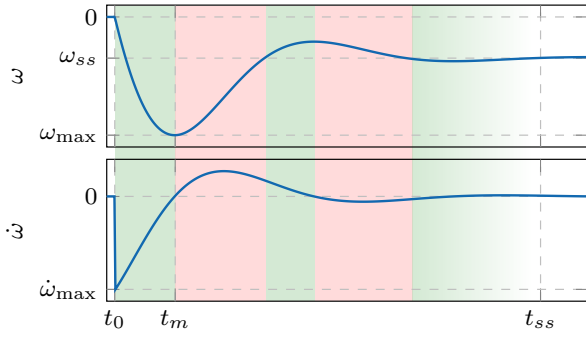


Fig. 2: Frequency response of a traditional power system. Shaded areas indicate the respective *accelerating* (green) and *decelerating* (red) intervals of the response.

machine. These phases are determined by the sign of the product ϱ , as follows:

$$\varrho(t) = \underbrace{(\omega(t) - \omega_{ss})}_{\Delta\omega(t)} \dot{\omega}(t) \begin{cases} > 0 & \mapsto \text{accelerating phase} \\ < 0 & \mapsto \text{decelerating phase} \end{cases}$$

which suggests that the same direction of frequency deviation and RoCoF would lead to an acceleration of the virtual machine and vice versa. Therefore, signal ϱ can be employed as a control input for adaptive regulation of the converter control gains, more specifically M_c and D_c for VSM and R_c for droop-based converters. For simplicity, we will solely focus on the former control strategy in this study.

B. Existing Control Schemes

The beneficial aspects of the interval approach have first been emphasized in [11] with the proposition of a *bang-bang* (\mathcal{K}_{BB}) inertia control strategy, based on alternating the inertia constant of the VSM between two discrete values: the high value \overline{M}_c and the low value \underline{M}_c , while preserving the default, pre-disturbance damping D_c^* :

$$M_c(t) = \begin{cases} \overline{M}_c, & \forall t : \varrho(t) > 0 \\ \underline{M}_c, & \forall t : \varrho(t) \leq 0 \end{cases}, \quad D_c(t) = D_c^*$$

However, a single degree of freedom restricts the controller performance and the bang-bang characteristic leads to an oscillatory behavior. These issues have been addressed in [12], which extends on the concept by including the adaptive damping and a more practical control algorithm. Governed by the aforementioned notions of $\dot{\omega} \sim M^{-1}$ and $\Delta\omega \sim D^{-1}$, the so-called *self-adaptive* inertia and damping controller (\mathcal{K}_{SA}) improves on \mathcal{K}_{BB} by adjusting M_c and D_c proportionally to the respective RoCoF and frequency deviation:

$$M_c(t) = \begin{cases} M_c^* + k_M |\dot{\omega}(t)|, & \forall t : \varrho(t) > 0 \wedge |\dot{\omega}(t)| > \varepsilon_M \\ M_c^*, & \forall t : \varrho(t) \leq 0 \vee |\dot{\omega}(t)| \leq \varepsilon_M \end{cases}$$

$$D_c(t) = \begin{cases} D_c^* + k_D |\Delta\omega(t)|, & \forall t : \varrho(t) \leq 0 \wedge |\dot{\omega}(t)| > \varepsilon_D \\ D_c^*, & \forall t : \varrho(t) > 0 \vee |\dot{\omega}(t)| \leq \varepsilon_D \end{cases}$$

with k_M and k_D being the virtual inertia and damping feedback gains. Thresholds ε_M and ε_D are employed to cancel

out the adaptive components as soon as the system approaches equilibrium, thus preventing unwanted oscillations and instability. Nonetheless, while drastically better than the bang-bang approach, this strategy still preserves several inherent flaws such as: (i) the individual adaptive control of either inertia or damping, which is suboptimal for regulating the frequency nadir in (7); (ii) a discontinuous response resulting from a combination of the control scheme and a RoCoF-based threshold trigger.

C. Optimal Frequency-Constrained Control (\mathcal{K}_{OFC})

In this work, we improve on the existing strategies by simultaneously regulating the VSM control gains, which is justified by the fact that both M_c and D_c contribute to the limitation of frequency nadir during a disturbance. Furthermore, we aim at minimizing the necessary control effort, more precisely the energy utilization of the associated DC-side buffer, in order to keep the frequency within prescribed ENTSO-E thresholds: $\hat{\omega}_{\max} = 0.2$ Hz, $\hat{\omega}_{\min} = 1$ Hz/s [17]. This is achieved via a gain-scheduling approach, where the optimal VSM feedback gains (ΔM_c^* , ΔD_c^*) for the first *accelerating* phase, computed using Algorithm 1, are selected based on the measured disturbance ΔP , with T_c being a given time constant of the virtual machine. Subsequently, during the *decelerating* interval, the adaptive inertia component is neutralized, whereas the adaptive damping is set to decay with time as

$$\Delta D_c(t) = \frac{\Delta\omega(t)}{\omega_{\max} - \omega_{ss}} \Delta D_c^* + k_D \dot{\omega}(t) \quad (8)$$

and is limited within a range $[-D_c^*, \Delta D_c^*]$ such that the total damping $D_c(t)$ preserves a positive, decaying trend. Finally, the proposed adaptive VSM strategy is of the form:

$$M_c(t) = \begin{cases} M_c^* + \Delta M_c^*, & \forall t : \varrho(t) > 0 \wedge \mathcal{C}(\dot{\omega}(t), \ddot{\omega}(t)) \\ M_c^*, & \forall t : \varrho(t) \leq 0 \vee \neg \mathcal{C}(\dot{\omega}(t), \ddot{\omega}(t)) \end{cases}$$

$$D_c(t) = \begin{cases} D_c^* + \Delta D_c^*, & \forall t : \varrho(t) > 0 \wedge \mathcal{C}(\dot{\omega}(t), \ddot{\omega}(t)) \\ D_c^* + \Delta D_c(t), & \forall t : \varrho(t) \leq 0 \vee \neg \mathcal{C}(\dot{\omega}(t), \ddot{\omega}(t)) \end{cases}$$

with $\mathcal{C}(\dot{\omega}(t), \ddot{\omega}(t)) = |\dot{\omega}(t)| > \varepsilon_1 \wedge |\ddot{\omega}(t)| > \varepsilon_2$ representing the logical threshold based on RoCoF and its first derivative that ensures a smooth control transition. Although obtaining an accurate $\ddot{\omega}(t)$ measurement introduces a time delay, it does not hinder the control performance since both maximum RoCoF and nadir occur before the respective trigger activation.

Algorithm 1 Iterative computation of optimal control gains

- 1: Initialize $k = 0 \triangleright M_c^{(0)} = -\Delta P / \dot{\omega}_{\max}$, $D_c^{(0)} = M_c^{(0)} / T_c$
 - 2: **while** $\omega_{\max}^{(k)} < \hat{\omega}_{\max}$ **do**
 - 3: $k = k + 1$
 - 4: Update frequency nadir threshold in (7): $\triangleright \omega_{\max}^{(k)}$
 - 5: Marginal gain increase: $\triangleright M_c^{(k)} = M_c^{(k-1)} + \delta M_c$
 $\triangleright D_c^{(k)} = D_c^{(k-1)} + \delta D_c$
 - 6: **end while**
 - 7: Return $\Delta M_c^* = M_c^{(k)} - M_c^*$, $\Delta D_c^* = D_c^{(k)} - D_c^*$
-

D. Stability Assessment

In this section, we focus on deriving the sufficient stability conditions for adaptive VSM design. Based on the Lyapunov stability theorem, the stability of the system is guaranteed if the following tuning conditions are included in Algorithm 1:

$$\begin{aligned} \Delta M_c^* &\leq 2M + 2(D + F_g)T \\ \Delta D_c^* &\geq 2\frac{M}{T} - 2(D + F_g) \end{aligned} \quad (9)$$

Proof. We start the proof by finding an appropriate candidate Lyapunov function of a nonlinear open-loop system. Similar to the stability analysis of a synchronous generator in [18], we obtain the respective energy function from the state-space representation of the system as follows:

$$\begin{aligned} V &= \int_0^{\dot{\omega}} M\dot{\omega}d\dot{\omega} + \frac{1}{T} \int_{\omega_{ss}}^{\omega} ((D + R_g)\omega - \Delta P)d\omega \\ &= \frac{1}{2}M\dot{\omega}^2 - \frac{1}{T}[\Delta P(\omega - \omega_{ss}) - \frac{1}{2}(D + R_g)(\omega^2 - \omega_{ss}^2)] \end{aligned} \quad (10)$$

where $V(\omega, \dot{\omega})$ represents the transient energy of the system in $(\omega, \dot{\omega})$ coordinates after a step disturbance ΔP . It can easily be shown that the proposed Lyapunov function has a stationary point at the system equilibrium i.e., $\nabla V(x^*) = 0$, as well as that it is positive definite in the vicinity of that equilibrium point, thus validating V as an appropriate Lyapunov candidate function. In order to guarantee stability in a closed-loop form, $\dot{V} = \partial V/\partial t$ has to be negative semi-definite $\forall t \in [0, \infty)$:

$$\begin{aligned} \dot{V} &= \frac{\partial V}{\partial \dot{\omega}} \frac{\partial \dot{\omega}}{\partial t} + \frac{\partial V}{\partial \omega} \frac{\partial \omega}{\partial t} + \frac{\partial V}{\partial M} \frac{\partial M}{\partial t} + \frac{\partial V}{\partial D} \frac{\partial D}{\partial t} \\ &= -\left(\frac{M}{T} + D + F_g\right)\dot{\omega}^2 + \underbrace{\frac{1}{2} \frac{\partial M}{\partial t} \dot{\omega}^2}_{\nu_M(t)} + \underbrace{\frac{1}{2T} \frac{\partial D}{\partial t} (\omega^2 - \omega_{ss}^2)}_{\nu_D(t)} \end{aligned} \quad (11)$$

which is conservatively subsumed in $\nu_M(t) + \nu_D(t) \leq 0$, $\forall t \in [0, \infty)$. The non-smooth characteristic of $\nu_M(t)$ and $\nu_D(t)$ can be resolved by observing different segments of the response indicated in Table I, and subsequently approximating $\partial M/\partial t$ by its average value at the points of switching, i.e., $\Delta M_c^*/T$, which implies the first condition in (9). Furthermore, it suggests that ensuring $\dot{\nu}_D(t) \leq 0$ after the frequency nadir has been reached would guarantee stability, thus resulting in an inequality condition of the form:

$$\dot{\nu}_D(t) = \frac{1}{2T} \frac{\Delta D_c^*}{\omega_{\max} - \omega_{ss}} \dot{\omega}(t)(\omega(t)^2 - \omega_{ss}^2) \leq 0 \quad (12)$$

with the damping component $k_D \dot{\omega}(t) \approx 0$ considered negligible. Since $\dot{\omega}(t)$ and $(\omega_{\max} - \omega_{ss})$ terms are of opposite sign, the

TABLE I: Values of ν_M and ν_D throughout the response.

Interval	$\nu_M(t)$	$\nu_D(t)$
pre-disturbance	$0 \mapsto (\partial M/\partial t = 0)$	$0 \mapsto (\partial D/\partial t = 0)$
disturbance	$> 0 \mapsto (\partial M/\partial t \uparrow)$	$0 \mapsto (\omega^2 - \omega_{ss}^2 \approx 0)$
pre-nadir	$0 \mapsto (\partial M/\partial t = 0)$	$0 \mapsto (\partial D/\partial t = 0)$
nadir	$0 \mapsto (\partial \omega/\partial t \approx 0)$	$0 \mapsto (\partial D/\partial t = 0)$
post-nadir	$0 \mapsto (\partial M/\partial t = 0)$	$\dot{\nu}_D(t)$

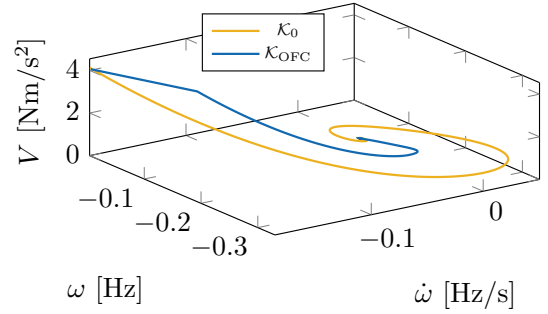


Fig. 3: Transient energy trajectory after a step disturbance.

problem in (12) corresponds to $|\omega(t)| \geq |\omega_{ss}|$, i.e., the system being critically damped or overdamped throughout the post-nadir interval. Mathematically speaking, the damping ratio in (3) must suffice $\zeta(t) \geq 1$, $\forall t \in [t_m, \infty)$. Having in mind that during this interval $\partial D/\partial t < 0$ and $T \geq M/D(t)$, as well as $R_g \approx F_g$, one can observe that $\zeta(t)$ is a decaying function:

$$\frac{\partial \zeta}{\partial t} = \sqrt{\frac{T}{M}} \frac{\partial D}{\partial t} \frac{TD(t) + T(2R_g - F_g) - M}{4(D(t) + R_g)^{3/2}} < 0$$

Therefore, combining $\zeta(t_m) \geq \zeta(t_{ss}) \geq 1$ with (3) yields the second stability condition in (9) and concludes the proof. ■

The results shown in Fig. 3 confirm that $V(\omega, \dot{\omega})$ remains positive, with transient energy trajectory preserving a decaying trend throughout the disturbance period and converging to the same equilibrium as the open-loop VSM approach (\mathcal{K}_0).

E. System Modeling and Control Implementation

The proposed adaptive VSM controller is implemented within a state-of-the-art VSC control scheme previously described in [19]. The outer control loop consists of active and reactive power controllers providing the output voltage angle and magnitude reference by adjusting the predefined setpoints according to a measured power imbalance. Subsequently, the reference voltage vector is passed through a virtual impedance block, as well as the inner control loop consisting of cascaded voltage and current controllers. The output is combined with the DC-side voltage in order to generate the modulation signal. The complete mathematical model consists of 13 states, and is implemented in a rotating (dq)-frame and per unit. More details on the overall converter control structure, employed parametrization, potential operation modes and respective transient properties can be found in [14], [16], [19].

For synchronous generators, we consider a traditional model equipped with a prime mover and a *TGOVI* governor. Furthermore, the automatic voltage regulator based on a simplified excitation system *SEXS* is incorporated, together with a *PSSIA* power system stabilizer [20]. Internal machine dynamics are characterized by the flux linkage dynamics of the rotor circuits, which together with 6 controller states and swing equation dynamics yield a standard 12th order system [21].

IV. RESULTS

As proof of concept, we test the proposed control design on a modified version of the well investigated Kundur's 2-

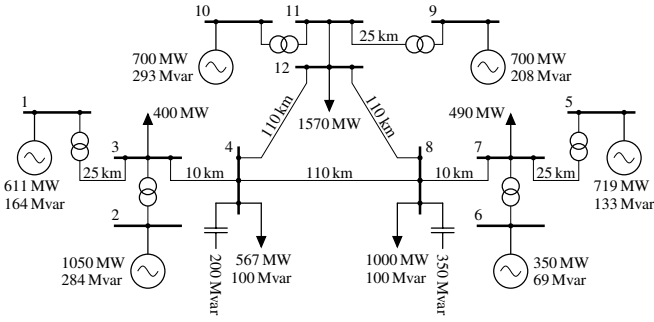


Fig. 4: Topology of the investigated 3-area test system: the converter-based generation is placed at nodes 2, 6 and 10.

area system illustrated in Fig. 4, comprised of 3 areas and 6 generators. The same test case has been previously used in several studies on placement and effects of inertia and damping in low-inertia systems [22], [23]. Furthermore, we consider a scenario where three traditional generators are replaced with converter-based units, and simulate a 100 MW load increase at node 12 using a detailed time-domain model developed in MATLAB Simulink. For clarity, only the center-of-inertia frequency is presented in this section.

The system response under different VSM control designs is depicted in Fig. 5. Understandably, the investigated contingency leads to unacceptable frequency excursion under the open-loop control \mathcal{K}_0 , indicated by the frequency nadir of 0.33 Hz. While \mathcal{K}_{BB} and \mathcal{K}_{SA} reduce this deviation, it is still kept above the admissible ENTSO-E threshold. On

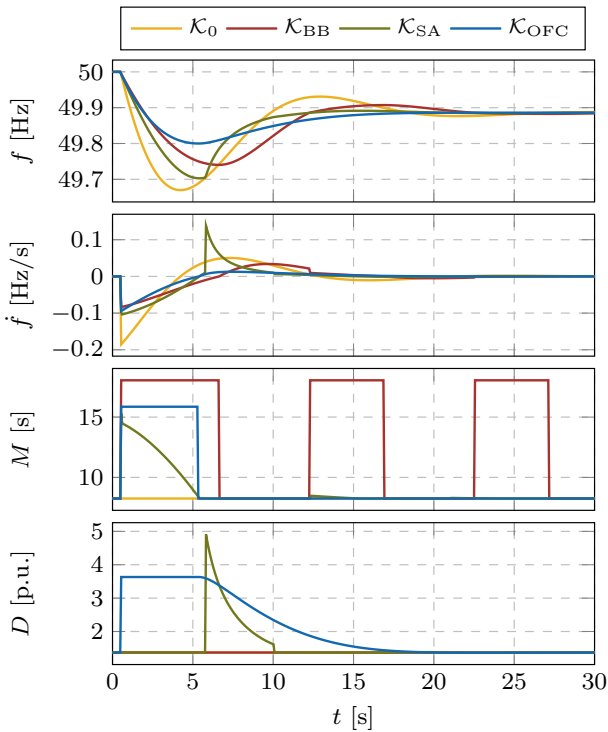


Fig. 5: System response under different VSM control designs: (i) frequency; (ii) RoCoF; (iii) inertia; (iv) damping.

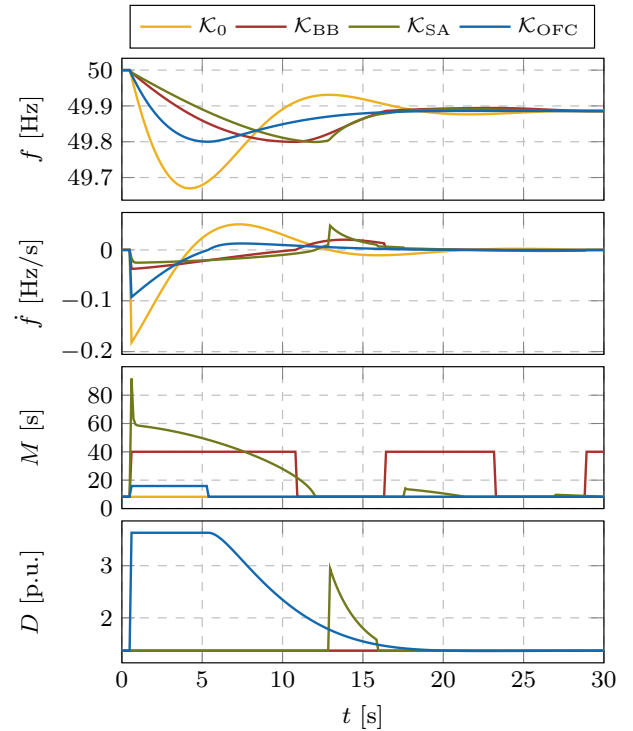


Fig. 6: System response under different VSM control designs, retuned such that they meet the prescribed ENTSO-E criteria: (i) frequency; (ii) RoCoF; (iii) inertia; (iv) damping.

the other hand, \mathcal{K}_{OFc} ensures that the frequency nadir is preserved within the given bounds, and provides the smoothest response; \mathcal{K}_{BB} has a high settling time due to insufficient damping, whereas the \mathcal{K}_{SA} is characterized by a discontinuity at the instance of frequency nadir. Moreover, the latter designs are inherently suboptimal, as they presume independent and inefficient temporal regulation of either inertia or damping. More precisely, \mathcal{K}_{BB} tends to activate high levels of inertia at wrong time instances, leading to a sluggish response, whereas \mathcal{K}_{SA} control strategy increases damping when ω is at its peak, resulting in the aforementioned power spike. In contrast, the proposed VSM approach immediately employs both the proportional (D) and derivative (M) control gains for preserving frequency within the given bounds. The efficiency of such approach can be observed in Fig. 6, with the inertia gains of \mathcal{K}_{BB} and \mathcal{K}_{SA} retuned such that $\omega_{\max} = 0.2$ Hz. As a result, the swing time constant $T = M/D$ increases, which makes up for a very high control effort and an unacceptably slow response.

Some insightful conclusions regarding the described control schemes can be drawn from the energy content of the control effort presented in Fig. 7, with respective energy terms computed as $\Delta E_M = \int \Delta M \dot{\omega} dt$ and $\Delta E_D = \int \Delta D \omega dt$. First of all, it justifies the proposed concept of compensating inertia with damping during high RoCoF instances, since the ΔE_M term would have a predominant impact on the total energy utilization. Moreover, it can be observed that \mathcal{K}_{OFc} reduces the total energy of the adaptive control by 20% and 40% compared to \mathcal{K}_{BB} and \mathcal{K}_{SA} , respectively. Moreover, it

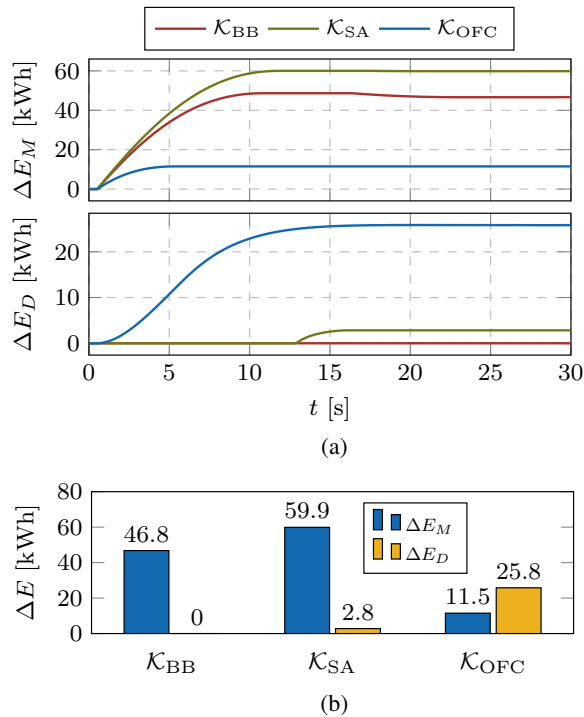


Fig. 7: Energy utilization for containing the frequency within limits: (a) activation of individual control components over time; (b) total contribution of additional control effort.

predominantly employs the proportional droop-like response, with ΔE_D contributing to 70% of the total energy. The activation of individual control components in Fig. 7a reveals the distinctive nature of the three algorithms. The existing interval-based controllers are restricted solely to adaptive inertia as a mean of frequency regulation during the initial response, which directly acts on RoCoF through the explicit $M\dot{\omega}$ term. The effectiveness of such approach is however limited, since the impact of inertia decays over time, together with $\dot{\omega}$. As a result, the inertia gain is overdimensioned, leading to high depletion of energy. In contrast, the combined effort of inertia and damping in \mathcal{K}_{OFc} achieves a qualitatively similar system performance with a more natural frequency response and less energy consumption. We therefore conclude that \mathcal{K}_{OFc} is both a more efficient and practical approach for adaptive VSM design.

V. CONCLUSION

The presented paper introduces a novel distributed VSM concept for converters in power systems with high shares of renewable resources. Using an interval-based approach, the emulated inertia and damping constants are adaptively adjusted according to the frequency disturbance in the system, while simultaneously preserving stable operation and frequency within prescribed limits. The proposed control design is integrated into a state-of-the-art converter control and compared against the existing VSM approaches, showcasing a superior performance in terms of frequency regulation and energy utilization. It is verified that the simultaneous control of both inertia and damping throughout the whole system response achieves a

drastically smoother frequency characteristic at a lower cost. Future work will focus on improving the optimality of the control design, as well as extending it onto no-inertia power systems.

REFERENCES

- [1] A. Ulbig, T. S. Borsche, and G. Andersson, "Impact of low rotational inertia on power system stability and operation," *IFAC Proceedings Volumes*, vol. 47, no. 3, pp. 7290 – 7297, 2014.
- [2] J. Rocabert, A. Luna, F. Blaabjerg, and P. Rodriguez, "Control of power converters in ac microgrids," *IEEE Transactions on Power Electronics*, vol. 27, no. 11, pp. 4734–4749, Nov 2012.
- [3] Q. C. Zhong and G. Weiss, "Synchroverters: Inverters that mimic synchronous generators," *IEEE Transactions on Industrial Electronics*, vol. 58, no. 4, pp. 1259–1267, April 2011.
- [4] M. Ashabani and Y. A. R. I. Mohamed, "Novel comprehensive control framework for incorporating vscs to smart power grids using bidirectional synchronous-vsc," *IEEE Transactions on Power Systems*, vol. 29, no. 2, pp. 943–957, March 2014.
- [5] J. Fang, X. Li, and Y. Tang, "Grid-connected power converters with distributed virtual power system inertia," in *2017 IEEE Energy Conversion Congress and Exposition (ECCE)*, Oct 2017, pp. 4267–4273.
- [6] J. Morren, S. W. H. de Haan, W. L. Kling, and J. A. Ferreira, "Wind turbines emulating inertia and supporting primary frequency control," *IEEE Trans. Sustainable Energy*, vol. 21, no. 1, pp. 433–434, Feb 2006.
- [7] N. Soni, S. Doolla, and M. C. Chandorkar, "Improvement of transient response in microgrids using virtual inertia," *IEEE Transactions on Power Delivery*, vol. 28, no. 3, pp. 1830–1838, July 2013.
- [8] M. A. T. L., L. A. C. Lopes, L. A. M. T., and J. R. E. C., "Self-tuning virtual synchronous machine: A control strategy for energy storage systems to support dynamic frequency control," *IEEE Transactions on Energy Conversion*, vol. 29, no. 4, pp. 833–840, Dec 2014.
- [9] U. Markovic, Z. Chu, P. Aristidou, and G. Hug, "Fast frequency control scheme through adaptive virtual inertia emulation," in *2018 IEEE Innovative Smart Grid Technologies - Asia (ISGT-Asia)*, May 2018.
- [10] U. Markovic, Z. Chu, P. Aristidou, and G. Hug, "LQR-based adaptive virtual synchronous machine for power systems with high inverter penetration," *IEEE Trans. Sustainable Energy*, 2019 (forthcoming).
- [11] J. Alipoor, Y. Miura, and T. Ise, "Power system stabilization using virtual synchronous generator with alternating moment of inertia," *IEEE Journal of Emerging and Selected Topics in Power Electronics*, vol. 3, no. 2, pp. 451–458, June 2015.
- [12] D. Li, Q. Zhu, S. Lin, and X. Y. Bian, "A self-adaptive inertia and damping combination control of vsg to support frequency stability," *IEEE Transactions on Energy Conversion*, vol. 32, no. 1, pp. 397–398, March 2017.
- [13] P. M. Anderson and M. Mirheydar, "A low-order system frequency response model," *IEEE Transactions on Power Systems*, vol. 5, no. 3, pp. 720–729, Aug 1990.
- [14] U. Markovic, O. Stanojev, P. Aristidou, and G. Hug, "Partial grid forming concept for 100% inverter-based transmission systems," in *IEEE PES General Meeting*, Aug 2018.
- [15] U. Tamrakar, D. Shrestha, M. Manisha, B. P. Bhattarai, T. M. Hansen, and R. Tonkoski, *Virtual Inertia: Current Trends and Future Directions*. MDPI AG, June 2017.
- [16] R. Ofir, U. Markovic, P. Aristidou, and G. Hug, "Droop vs. virtual inertia: Comparison from the perspective of converter operation mode," in *2018 IEEE International Energy Conference (ENERGYCON)*, June 2018.
- [17] ENTSO-E, "Frequency stability evaluation criteria for the synchronous zone of continental europe," Tech. Rep., March 2016.
- [18] J. Machowski, J. W. Bialek, and J. R. Bumby, *Power System Dynamics: Stability and Control*. Wiley, 2008.
- [19] U. Markovic, J. Vorwerk, P. Aristidou, and G. Hug, "Stability analysis of converter control modes in low-inertia power systems," in *2018 IEEE Innovative Smart Grid Technologies - Europe (ISGT-Europe)*, Oct 2018.
- [20] ENTSO-E, "Documentation on controller tests in test grid configurations," Tech. Rep., November 2013.
- [21] P. Kundur, *Power System Stability and Control*. McGraw-Hill, 1994.
- [22] T. S. Borsche, T. Liu, and D. J. Hill, "Effects of rotational inertia on power system damping and frequency transients," in *2015 54th IEEE Conference on Decision and Control (CDC)*, Dec 2015.
- [23] D. Groß, S. Bolognani, B. Poolla, and F. Dörfler, "Increasing the resilience of low-inertia power systems by virtual inertia and damping," in *IREP Bulk Power System Dynamics & Control Symposium*, Aug 2017.